Radar, signal, and image processing techniques for through the wall imaging

Moeness G. Amin

Center for Advanced Communication
Villanova University
Villanova, Pa 19085

ABSTRACT

In this paper, we discuss some of the leading issues in through the wall radar imaging (TWRI) problems. We focus on the primary system challenges and deliverables, dealing only with the applications of statistical signal and array processing. Applications of antenna design and electromagnetic propagation are equally important, but they are both outside the scope of this paper. The material presented considers key desirable TWRI system properties and features and provides candidate solutions to achieve them. We focus on research performed at Villanova University and demonstrate some of our recent approaches to address system functionalities and requirements using analyses, computer simulations, and real-data. The paper does not attempt to cover all progress made in the field to date nor does it intend to compare the proposed techniques with alternative and competitive methods. It is written with the primary purpose of bringing to the reader many leading challenges and diverse issues worthy of considerations.

Keywords: imaging, array processing, through the wall, wideband beamforming, auto-focusing, step-frequency.

1. INTRODUCTION

 "Seeing" the targets behind obstacles such as walls, doors, and other visually opaque materials, using microwave signals is considered as a powerful tool for a variety of applications in both military and commercial paradigms. Through-the-wall Radar imaging (TWRI) has been recently sought out in rescue missions, behind-the-wall target detection, surveillance and reconnaissance. There are several studies on TWRI to detect targets and the presence of persons behind walls and track their movements with known wall and unknown parameters, such as wall thickness and dielectric constant [1-12].

The TWRI is a complex and difficult problem that requires cross-disciplinary research in electrical engineering. Fundamentally, it is a hybrid between two main areas, statistical signal, radar, and array processing on one hand and antennas and electromagnetics on the other. There are many challenges facing Through the Wall Radar Imaging system developments, namely, the system should be reliable, portable, light weight, small-size, and has both short acquisition time and set-up time. The system performance should be robust to ambiguities and inaccuracies in wall parameters and should properly function under non-uniform wall, multiple walls, and operator motion. Ultimately, the system should have high range and cross range resolutions, which could be application specific. Finally, the TWRI system must be able to detect and classify motions in a populated scene and in the presence of heavy clutter, which may include interior back and side walls, water pipes, electrical cords, and various types of furniture items.

There are two different approaches to Through-the-Wall Radar Imaging. The first approach is coherent imaging that requires wideband beamforming to be applied, using multiple antenna transmitter and receiver arrays. Measurements should include the data magnitude and phase to be used in post-data processing for imaging each pixel behind the wall. The non-coherent approach involves several, more simplified and stand-alone radar units. In this case, imaging is performed based on the trilateration technique, which is a method to determine the position of an object based on range measurements (obtained from time-of-arrival information) from three radar units located at known sites. The three radar units can be monostatic, bistatic, or a combination of both. The range measurements are used to form constant-range contours (ellipses for bistatic and circles for monostatic configurations) with foci at the respective radar locations. The common intersection point of the three contours is the target location [13]. For both of the above approaches, we use the stepped-frequency scheme, which achieves the same result as the one based on ultra wideband pulse, while avoiding the

difficulties arising from using short time duration signal and increased complexity of transmitter and receiver hardware design. Further, the step-frequency implementation allows changing the emitted power over signal bandwidth. We can, therefore, compensate for the frequency-dependent power attenuation of the wall, limiting the signal time-dispersion and preserving the shape of the intended pulse as it travels through the wall.

In this paper, we discuss key techniques that contribute to solving the TWRI problem from the signal and array processing perspectives. The material presented is a summary of recent efforts made by the TWRI research team at the Center for Advanced Communications at Villanova University. We have considered both coherent and noncoherent approaches. The research focus has been on two aspects of the problem, leading to requiring few antennas and imaging under unknown wall characteristics. While the former is obviously attractive for cost and simplicity reasons, the latter is important, so that undistorted, high quality imaging can be obtained. Large errors in wall parameters cause smearing of the image and displace targets away from their true positions. These effects reduce the accuracy of the TWRI and compromise the integrity and main objectives of the system.

2. WIDEBAND BEAMFORMING

Consider an M-element transmit and an N-element receive line array, both located along the x-axis. Let the transmitter, placed at the m-th transmit location $\mathbf{x_{tm}}$, illuminate the scene with a wideband signal $s(t)$. The reflection by any target is measured and stored by the receiver at the n-th receive location $\mathbf{x_{rn}}$. For the case of a single point target located at $\mathbf{x_p}=(x_p,z_p)=(R_p\sin\theta_p, R_p\cos\theta_p)$, the output of the n-th receiver is given by $a(\mathbf{x_p})s(t\text{-}\tau_{mn})$, where $a(\mathbf{x_p})$ is the complex reflectivity of the point target. As shown in Fig.1, the propagation delay τ_{mn}, encountered by the signal as it travels from the m-th transmitter to the target and back to the n-th receiver, is

$$\tau_{mn} = \frac{d(\mathbf{x_{tm}},\mathbf{x_p})}{c} + \frac{d(\mathbf{x_p},\mathbf{x_{rn}})}{c} \tag{1}$$

where c is the speed of light and $d(\mathbf{x},\mathbf{y})$ denotes the Cartesian distance between locations $\mathbf{x}$ and $\mathbf{y}$.
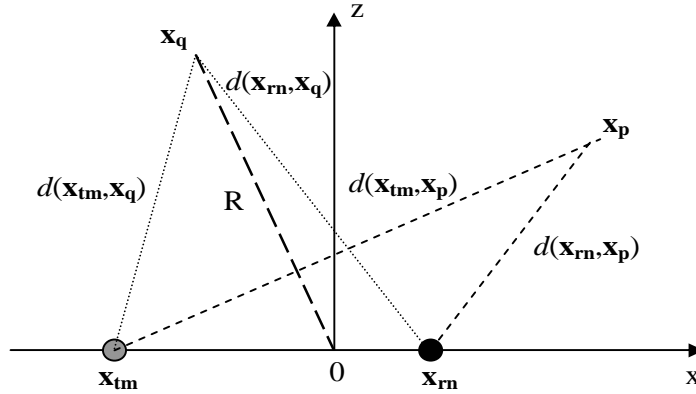

Figure 1. Geometrical description

The above process is repeated, with the transmitter at the m-th location, until all N receive locations have been used sequentially. The corresponding N outputs are processed as follows. The region of interest is divided into a finite number of pixels in range and angle. As shown in the system block diagram of Fig. 2, the complex composite signal corresponding to the image of the pixel located at $\mathbf{x_q}$ (at range R_q in the direction θ_q), is obtained by applying time delays and weights to the outputs of the N receivers, and summing them. The resulting output for a single target case is given by

$$z_{mq}(t) = \sum_{n=1}^{N} w_{rn}a(\mathbf{x_p})s(t - \tau_{mn} - \tilde{\tau}_{mn}) \tag{2}$$

where w_{rn} is the weight applied to the output of the n-th receiver. The parameter, $\tilde{\tau}_{mn}$, is the focusing delay applied to the output of the n-th receiver when the transmitter is at the m-th location,

$$\tilde{\tau}_{mn} = \frac{2R_q}{c} - \frac{d(\mathbf{x_{tm}},\mathbf{x_q})}{c} - \frac{d(\mathbf{x_q},\mathbf{x_{rn}})}{c} \tag{3}$$

The focusing delay synchronizes the arrivals at different receive locations for the same pixel, and as such allows coherent imaging of the scene. If $\mathbf{x_p}=\mathbf{x_q}$, then all signal arrivals assume the same delay $2R_q/c$, which corresponds to the time of flight of the wideband waveform for the focused range R_q. The above process is repeated by sequential use of the M transmit locations and produces M complex composite signals, $z_{mq}(t)$, $m=1,2,\ldots M$, corresponding to the image of the pixel at $\mathbf{x_q}$. The final complex signal corresponding to the pixel located at $\mathbf{x_q}$ is obtained by the coherent weighted linear combination given by [10]

$$z_q(t) = \sum_{m=1}^{M} w_{tm} z_{mq}(t) = \sum_{m=1}^{M}\sum_{n=1}^{N} w_{tm}w_{rn}a(\mathbf{x_p})s(t-\tau_{mn}-\tilde{\tau}_{mn}) \tag{4}$$

where w_{tm} is the weight applied to the component signal $z_m(t)$ obtained using the m-th transmitter. The complex amplitude image value for the pixel located at $\mathbf{x_q}$ is

$$I(\mathbf{x_q}) = z_q(t)\Big|_{t=\frac{2R_q}{c}} \tag{5}$$

The above process is performed for all pixels to generate the composite image of the scene. The general case of multiple targets can be obtained by superposition.
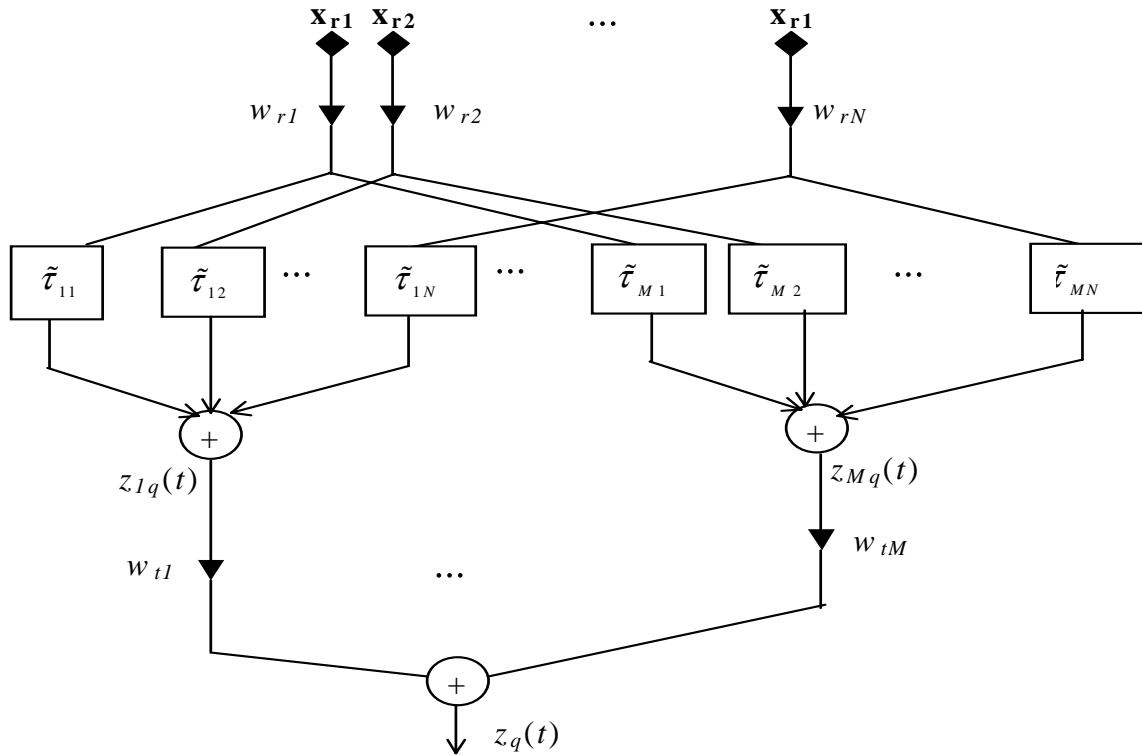

Figure 2: Block diagram of the post-data acquisition beamformer

The composition and thickness of the wall, its dielectric constant, and the angle of incidence affect the strength and characteristics of the signal propagating through the wall. The loss of signal power and slowing down and bending of the wave as it propagates through a dielectric medium are important factors that must be taken into account for effective and accurate imaging. Failure to do so would result in significant errors in setting the focusing delays $\tilde{\tau}_{mn}$, which in turn cause undesirable errors in determining the nature and the locations of the targets. These errors increase in the presence of walls with high dielectric constants such as concrete [13].

3. EFFICIENT IMPLEMENTATIONS VIA MULTIPLEXING

Due to the linear processing underlying the above operation, the number of designated processors can be reduced to two; one designated to the transmitters and the other is the receivers. We use multiplexing to deliver the proper time delays for each mode, as shown in Fig.3.
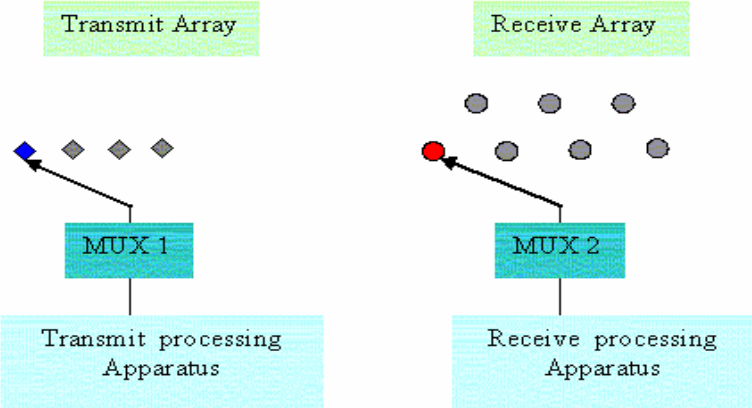
Figure 3   Multiplexing modes

Figure 2 shows how to reduce the number of processors, but not the number of antennas. The latter can be reduced to only be using one transmitter antenna and one receive antenna. For example, the "blue" and the "red" antennas can be both moved to new specified positions in the array upon completion of scanning all pixels. As depicted in Fig.4, the system simplifies to two-antenna requirements, contingent to the ability for sensor-relocation along with cascade data collection.

Figure 4. Two-Antenna Requirement

4. SIMPLIFIED SYNTHETIC APERTURE PROCESSING USING CO-ARRAYS

The use of two-antenna TWRI, according the above discussions, does not alter the aperture or reduce it. The number of different locations of the antennas remains the same, independent of whether the implementation of Fig. 3 or 4 is adopted. Improved spatial resolution can be achieved by using an enlarged array aperture. However, with the constraints of portability and low cost on the system, an innovative scheme is required for increasing the effective system aperture. In the proposed TWRI system, we use an aperture synthesis scheme based on the co-array formalism. The concept of co-arrays was originally defined for narrow-band far-field active imaging, and has also been extended to wideband imaging. The co-array provides a convenient and elegant framework for understanding linear imaging techniques [14]. The co-array

completely characterizes the performance of an imaging system, and is defined to be the set

$$C_S = \{ \underline{z} : \underline{z} = \underline{x} + \underline{y}, \underline{x} \in S_T, \underline{y} \in S_R \} \qquad (6)$$

where ST and SR are the sets containing the position vectors of the elements in the transmit and receive apertures, respectively. It is possible for two systems that have the same coarray to achieve the same imaging performance. Figure 5 shows the co-arrays for 1-D and 2-D settings. It is clear that the number of antennas and the extent of the transmit and receive arrays is smaller than the Sum co-array with shared spatial resolution.
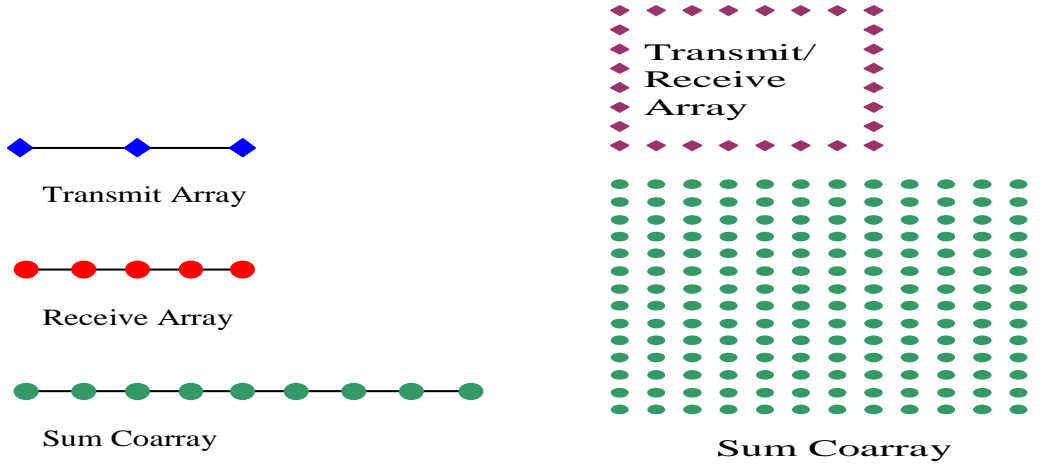

Figure 5. 1-D and 2-D Co-array examples

5. STEPPED-FREQUENCY APPROACH

Wideband signals, in the form of short duration pulses, are often used in active imaging to obtain range resolution. In order to achieve a high range resolution, a must-have feature for through-the-wall imaging systems, a relatively large bandwidth is required. However, this means that the pulse duration in time becomes rather short, thereby increasing the complexity of transmitter and receiver hardware design. We propose the stepped-frequency scheme for TWRI. This scheme achieves the same effect as that of short duration pulses while avoiding the difficulties of using short time duration signal [10].

The transmitted wideband signal $s(t)$ can be expressed in the frequency domain in terms of its Fourier transform $S(f)$. Instead of transmission and reception of the wideband pulse, one can transmit monochromatic signals corresponding to the continuum of frequencies constituting the wideband signal spectrum $S(f)$, measure the complex amplitude of the returns, and synthesize the wideband received waveform using corresponding spectral values $S(f)$.

A stepped-frequency approximation to the above approach would use a finite number, K, of monochromatic signals with equi-spaced frequencies, f_k, covering the desired bandwidth $f_{K-1} - f_0$. The complex amplitude image value of the q-th pixel, represented by eq. (5), can be expressed in terms of the stepped-frequency signal as

$$I(\mathbf{x_q}) = \sum_{k=0}^{K-1} S(f_k) \exp(j2\pi f_k t) a(\mathbf{x_p}) \sum_{m=1}^{M} \sum_{n=1}^{N} w_{tm} w_{rn} \exp(-j2\pi f_k (\tau_{mn} + \tilde{\tau}_{mn})) \Big|_{t=\frac{2R}{c}} \qquad (7)$$

$$f_k = f_0 + k\Delta f \; ; \quad \Delta f = \frac{f_{K-1} - f_0}{K-1} \qquad \text{for } k = 0, 1, \cdots, K-1$$

Here, Δf is the frequency step size. This expression forms the basis of the stepped-frequency implementation of the aperture synthesis scheme using subarrays. The time-delay $\tau_{mn} + \tilde{\tau}_{mn}$ now appears as a frequency dependent phase delay.

This implies that beamforming can be achieved by transmitting the K monochromatic signals with equi-spaced frequencies, measuring the complex amplitude of the returns, performing synthetic focusing in the frequency domain for each frequency using a phase delay corresponding to that frequency, and then combining the results per equation (7).

6. ROBUSTNESS TO WALL AMBIGUITIES

The errors in wall parameters typically impact the imaged target position more than its intensity profile. The shifts of targets away from their true positions depend on the errors in the wall parameters as well as the target locations with respect to the antenna array. Recently, a new approach to locate the target without the knowledge or estimation of the wall parameters has been introduced [15]. The wall is single and uniform. The transmit and receive arrays are assumed to have already been designed to meet the cross-range resolution specified by the system. Both arrays can be placed against the wall or at a standoff distance. A wideband pulse, with step-frequency implementations, meeting the required range resolution, is emitted by the transmit antennas and coherently combined at the receive antennas, using different sets of focusing delays corresponding to different image pixels. The approach requires imaging to be performed under at least two different array structures. For each array structure, imaging through the wall is obtained using multiple sets of assumed wall parameters. For each set, a trajectory, tracing the shift in the target location, is formed. The intersection of the trajectories, corresponding to the different array structures, is used as an estimate of the true target location.

To illustrate the target displacements due to wall ambiguities, consider three targets at different locations behind the wall. The transmit antennas and receive antennas are symmetric around their center point, and are placed against the wall. The transmit array consists of four antennas with inter-element spacing of 0.6 meter. The receive array consists of eight antennas with inter-element spacing 0.065 meter. Both the transmit and receive arrays are located along the x-axis at positions listed in Table 1. The wall thickness is $d = 0.4$ meter and the dielectric constant is $\varepsilon = 9$. The carrier frequency is 2 GHz and the pulse bandwidth is 1 GHz. The dielectric constant is assumed known, i.e., $\varepsilon_e = \varepsilon$, but the wall thickness assumes different values, $d_e = 0.6, 0.4, 0.2 \, m$. The second value is equal to the true wall thickness, whereas for the other values, $d_e \neq d$. The images corresponding to different pairs of wall parameters (ε, d_e) are superimposed. It is evident from Fig. 6 (a) that there are no significant changes in imaging qualities, even when the incorrect wall parameters are used. On the other hand, the targets are clearly shifted away from their true positions. The same behavior is observed if we use the correct wall thickness and perform imaging using different assumed values of the dielectric constant (See Fig. 6 (b)).
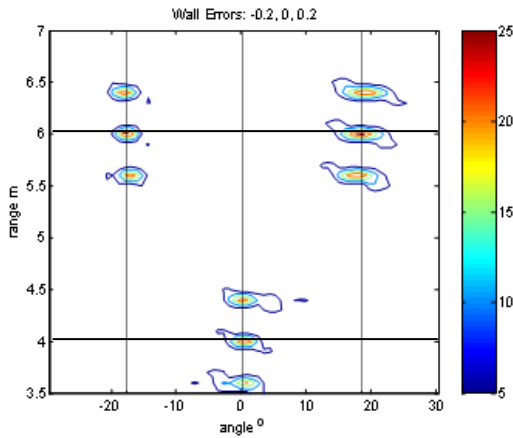

Fig. 6(a) Correct Dielectric Constant   Fig. 6(b) Correct Wall Thickness
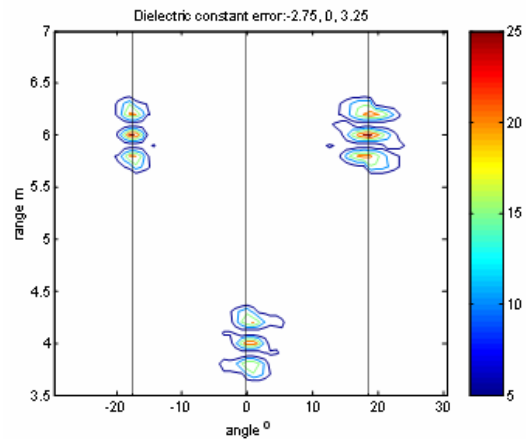
Element #	1	2	3	4	5	6	7	8

Transmit (m)	-0.9	-0.3	0.3	0.9				
Receive (m)	-0.2625	-0.1875	-0.1125	-0.0375	0.0375	0.1125	0.1875	0.2625
Table 1: Transmit and Receive array locations								

To solve the above problem and locate the target, we have proposed the following technique. Assume known wall dielectric constant. For one array structure, the trajectory of target displacements is obtained assuming different wall parameter values. Then, we shift the array parallel to the wall into a new position. We repeat the process and obtain a new trajectory. The intersection of the two trajectories is the target position. The proof of this argument is given in [16]. In the example below, we modify the antenna array structure of Table 1 by moving the transmit array 0.8 meter along the *x* axis, and generate another series of images. The images of targets follow the same moving pattern as in the original structure. However, because of the different locations of the transmit antennas in the two array structures, the respective target displacement trajectories are not identical. The intersection of the two trajectories provides the true target position and the true wall thickness. This is demonstrated by the simulation results shown in Fig. 7(a). In this figure, "." indicates the target image positions in angles for the original transmit array structure, whereas "*"indicates the target image positions in angles for the shifted transmit array structure.

The above argument and experiment can be extended to the case when the true wall thickness is known, but the dielectric constant is unknown. Trajectories, similar to those shown for the unknown wall thickness case, can be generated. Fig. 7(b) shows the simulation results of the two trajectories and their intersection point for this case.
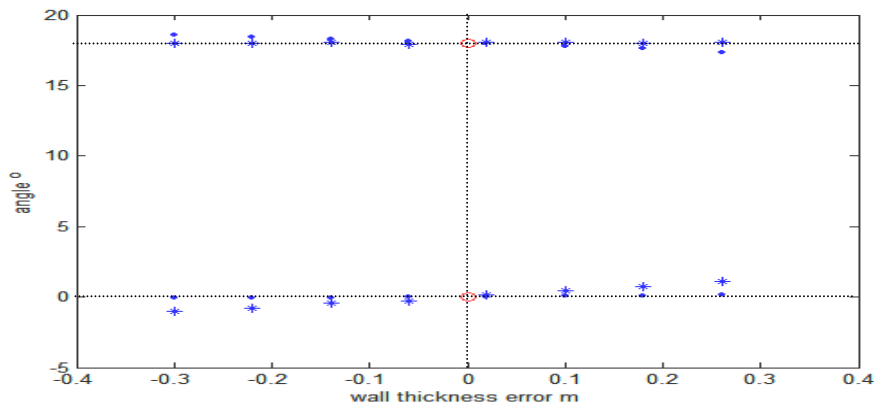
Fig. 7(a) Known dielectric constant
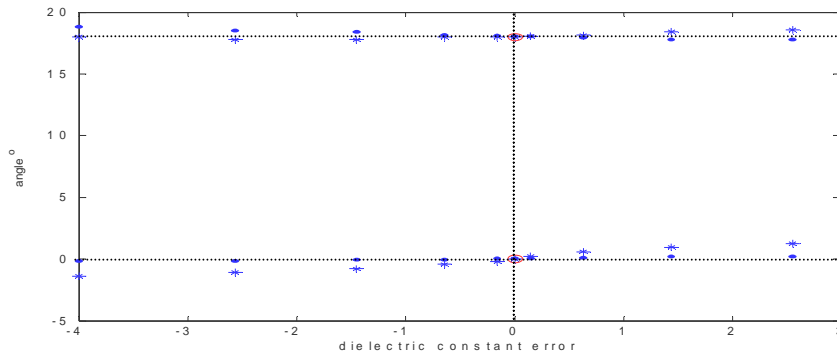
Fig. 7(b) Known wall thickness

7. AUTOFOCUSSING

As discussed in the previous section, not knowing the exact wall parameters can cause the target image to shift and blur. Although the shifting is more pronounced than blurring, we take in this section a different approach to combat wall ambiguities which is based on restoring image sharpness. The overall concept is captured in Fig. 8. It consists of a measuring module that would feedback the image quality using focusing metric to an adjustment module in which the wall parameters are tuned to reduce degradation. The proposed metrics successfully show a single, major peak at the correct wall parameters, but vary in the drop of the peak values when introducing slight wall errors.
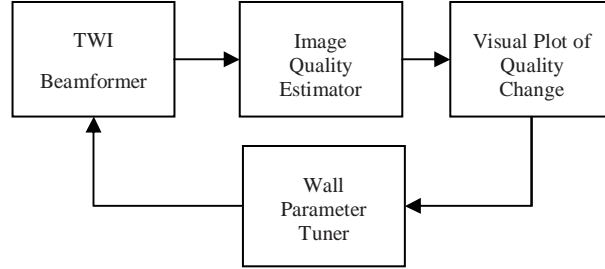

Fig. 8 Image Quality Adjustment Feedback Mechanism

The ruggedness of the two dimensional metric values with errors in wall thickness and dielectric constants make the application of the gradient search difficult, or impossible. Local gradient optimization algorithms are inadequate due to the high noise levels on the cost function surface. As such, it is difficult to automate the search for the highest peak value. It is assumed that the peak can be detected by the system operator.

Contrast optimization consists of changing various focus parameters of an image to maximize or minimize a contrast measure. Let ss(x,y) represent the value of the image intensity at point (x,y). The following criteria are commonly used as measures for image sharpness [17].

1) Normalized sum of image intensity

$$C_2 = \frac{\iint |ss(x,y)|^2 \, dxdy}{(\iint |ss(x,y)| \, dxdy)^2} \tag{8}$$

2) Normalized sum of squared intensity

$$C_3 = \frac{\iint |ss(x,y)|^4 \, dxdy}{(\iint |ss(x,y)| \, dxdy)^4} \tag{9}$$

3) Negative of Image Entropy

$$C_4 = \iint I(x,y) \ln[I(x,y)] dxdy \tag{10}$$

$$I(x,y) = \frac{|ss(x,y)|^2}{\iint ss(x,y) dxdy}$$

4) Ratio of Standard Deviation to mean amplitude

$$C_5 = \frac{\sqrt{\iint \left[|ss(x,y)| - \frac{1}{XY} \iint |ss(x,y) dxdy| \right]^2 dxdy}}{\iint |ss(x,y) dxdy|} \tag{11}$$

where X, Y are the total number of pixels along the x and y axes respectively. All integrals are performed over the extent of the image.

The above four metrics measure the "contrast" of the image. A good measure reaches a maximum or minimum value only for the undistorted image. If the contrast measures defined above tend to change monotonically with increasing errors in wall parameters, then we can reduce focusing errors by varying the estimates in a carefully-designed, controlled way to optimize image contrast. In [17], the above contrast measures are applied for TWRI. The underperformance of these measures in responding to errors in the wall characteristics has called for more robust and sensitive criteria, such as the higher order criteria Skewness and Kurtosis, estimated as

$$Skewness(\hat{\gamma}_3) = \frac{\sum_{i=1}^{N}(x_i - \hat{m})^3}{(N-1)\hat{\sigma}^3} \tag{12}$$

$$Kurtosis(\hat{\gamma}_4) = \frac{\sum_{i=1}^{N}(x_i - \hat{m})^4}{(N-1)\hat{\sigma}^4} - 3 \tag{13}$$

where $\hat{m}$ and $\hat{\sigma}$ denote the mean and the standard deviation over the N observations for the x_i (i=1, 2, 3…N). Another higher order metric (called Kurtosis ordered 'n' and denoted as kurtosis'n') is proposed, which is defined as follows,

$$\hat{\gamma}_n = \frac{\sum_{i=1}^{N}(x_i - \hat{m})^n}{(N-1)\hat{\sigma}^n} \tag{14}$$

The overhead using the higher order criteria is very evident in the drastic increase in the computations as the order increases. For a moderate order (ex.,15), it was observed that the sensitivity in the error change improved by over 200% compared to the contrast based measures.

In the simulation below, the true wall thickness is 12cms and the dielectric constant is 9. The wall thickness errors considered are from -12cms to +12cms from the true wall thickness value, for the case involving just wall errors. Due to space limitation, the case with both types of errors is not shown. It is evident from the plots in Fig. 9 that the higher order criteria outperform the contrast based metrics significantly in both the single target and two target cases.
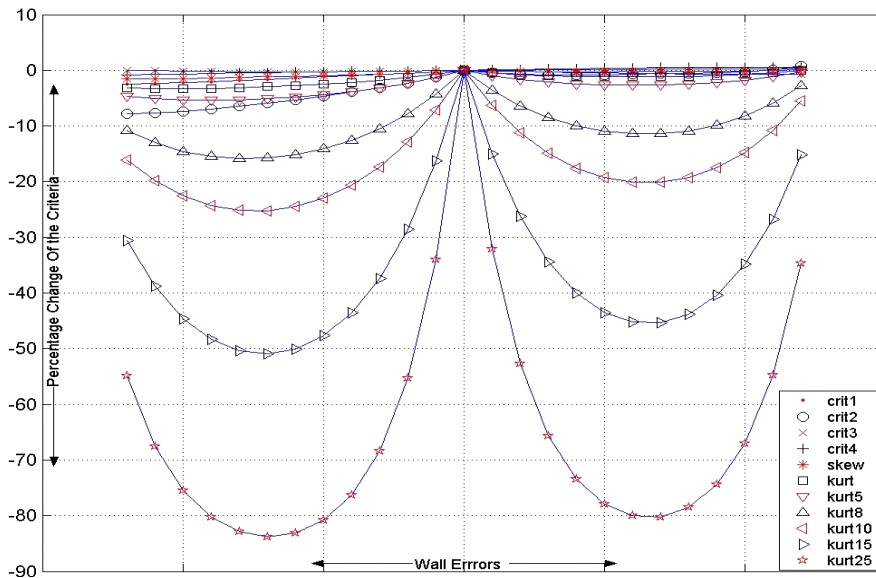

Fig 9 Percentage error change of the criteria involving just wall thickness errors in single target case

8. NON-COHERENT IMAGING

The non-coherent imaging is based on locating the target using range measurements from three or more radar units that operate independently. Figure 10 shows a schematic layout of the Communications Lab (Room 305, CEER Building) at Villanova University which is the room imaged using a non-coherent imaging approach. The lab contains computer equipment as well as metal storage units that resulted in very strong unwanted returns. We, therefore, opted for the following arrangement highlighted in the figure. The target will be placed at various locations in the lab and data acquired for each position. The planned target trajectory is as follows. The target will be moved towards the back wall, then along the back wall, and then away from the back wall moving towards the wall through which the radar system is looking, as shown in Fig. 10. The physical dimensions of the room being imaged, the antenna spacing, the stand-off distance, and the details of the target trajectory are specified in Fig. 11.
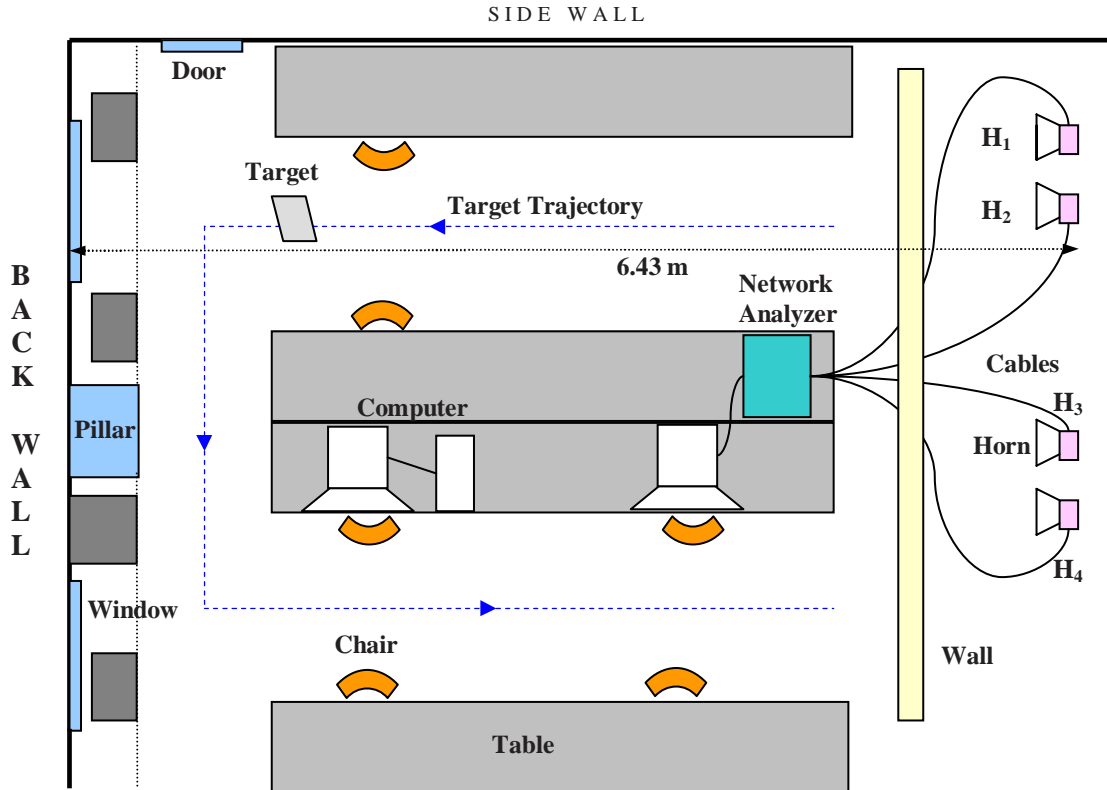
Figure 10. Schematic of the Communications Lab at Villanova University.

The four dark gray boxes along the back wall represent computer equipment.

A 7 GHz bandwidth stepped-frequency signal was used for imaging. The flat metal reflector was used, as the target and was moved to 23 different locations specified in Fig. 11. The target positions along the first and the last legs of the trajectory are equi-spaced, with a spacing of 2 ft, whereas the second leg has positions uniformly spaced at intervals of 1 ft. Four H-1479 horn antennas were used for signal transmission and reception. The exact antenna placement is provided in Figure 2. Note that not all of the target locations are in the fields of view of all four antennas. In the through-the-wall set up experiment, we employed a front wall, the cross-section of which is shown in Fig. 12 (plywood-air-drywall construction), placed 2 ft in front of the antenna baseline. For each target location, horn antennas (H_1, H_2, H_3, and H_4) were used to measure three sets of data, each corresponding to a different transmit/receive pair, i.e., different radar units (S_{21}, S_{32} and S_{43}, where S_{ij} is the set of data obtained using horn H_i as the receiver and horn H_j as the transmitter). Furthermore, the data measurement process for each transmit/receive pair consisted of the following steps:

- Background measurement: This is a time-domain measurement (using the time domain function of the Network Analyzer) of the envelope of the received stepped-frequency signal. The purpose of this experiment is to measure the characteristics of the lab, with only one exception; the target is not present.

- Target measurement: This is a time-domain measurement of the envelope of the received signal using the same exact setting as for the background measurement, but including the target.

- Background subtraction: The background data set is subtracted from the target data set for clutter reduction.

This final data set, after clutter subtraction, was used for range and cross-range processing. It is important to note that the system simplicity and flexibility, compared to those entailed in coherent processing, come at the expense of reduced performance.
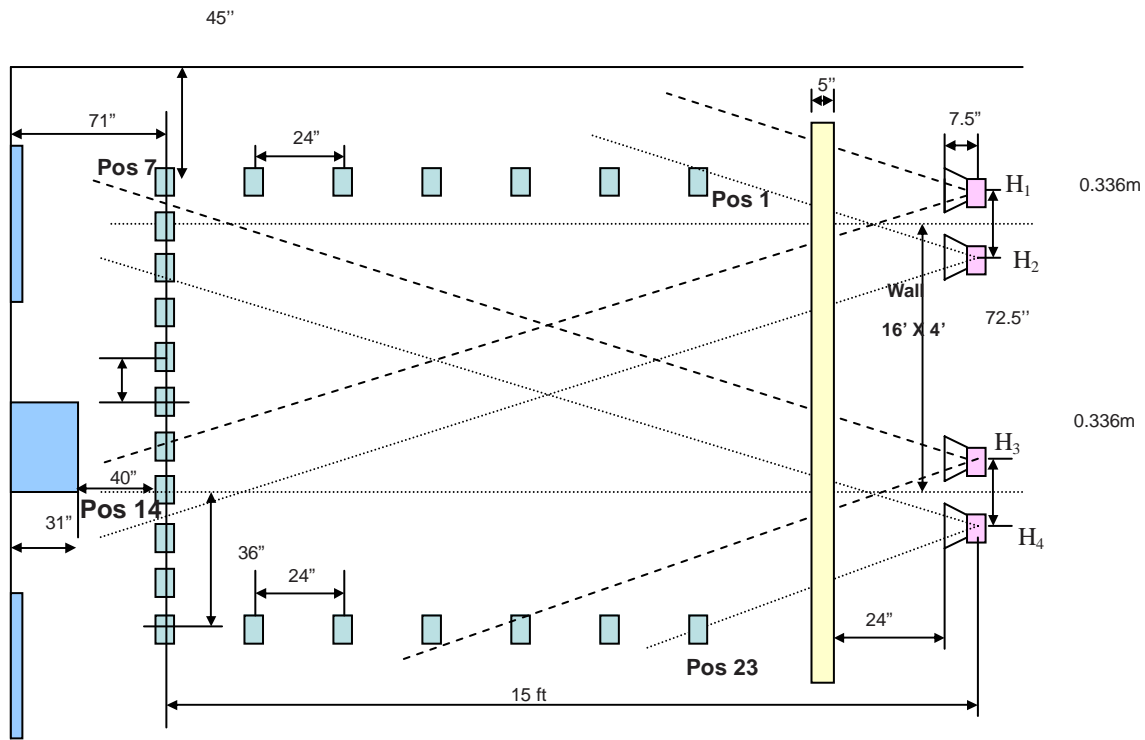

Fig.11 Diagram of the Experimental Setup in the Communications Lab at Villanova University.

The region of interest is divided into pixels in range and cross-range. The value assigned to the q-th pixel is computed as follows. We compute the time it would take the signal to travel from the transmitter, to the q-th pixel and then back to the receiver, for all three transmit/receive pairs, S_{21}, S_{32} and S_{43}, and label these delays as τ_{q21}, τ_{q32}, and τ_{q43} respectively. We then sample the three time-domain waveforms, corresponding to S_{21}, S_{32} and S_{43}, at time instants τ_{q21}, τ_{q32}, and τ_{q43} respectively. The q-th pixel is assigned a value equal to the sum of these sampled values. The image is generated by repeating this process until all the pixels in the region of interest have been exhausted.

The contour plot for position 14 is shown in Fig.13. We can clearly see three traces, one due to each of the transmit/receive pairs, intersecting very close to the target location. The slight error is a result of ignoring the wall effects, such as refraction and change in propagation speed, while processing the acquired data to produce the range vs. cross-range plot. Similar success was encountered for most of the target positions. At side target positions close to the wall, the target can be in the field of view of only two out of the three pairs of antennas. As such, only two clear traces

will be visible farther, depending on how close the target to the transmission wall, one trace may only be identified, rendering target localizations difficult and sometime impossible. This is the case for positions 1 and 23, shown in Fig. 11. This problem is not so much pronounced in coherent imaging.
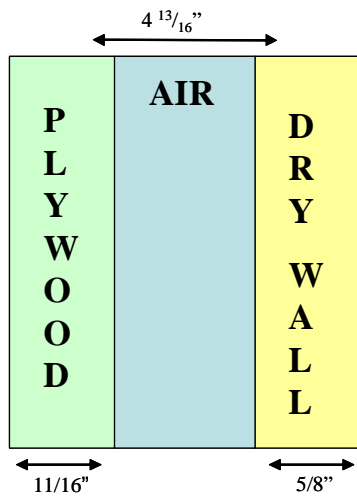

Fig. 12 Wall Characteristics
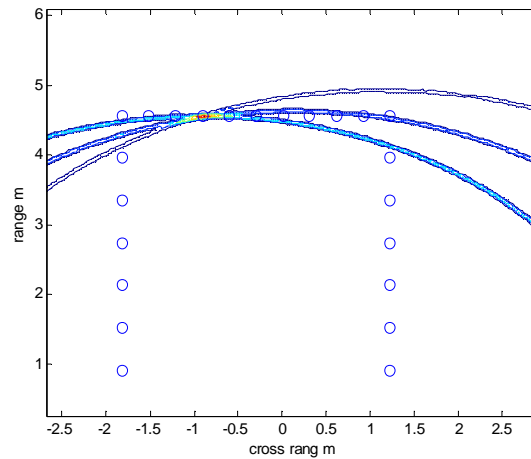
Fig. 13. Target location and contour plots

CONCLUSIONS

We have presented different methods, dealing with various challenges in developing and design a through the radar imaging system. The paper has reviewed wideband beamforming, as applies to TWRI and suggested implementations using step-frequency schemes. It has discussed two approaches to combat image impairments due to inaccuracies in wall parameters. The paper also touched on a method to reduce the number of antennas without sacrificing resolution. We have left out Doppler signature estimation and motion identification and tracking as well as we have not addressed the polarization difference imaging and its contribution to reduced clutter and improved target resolution. Further discussion on coherent and noncoherent approaches in the TWRI efforts at Villanova University can be found in references 18, 19.

REFERENCES

[1]   D. D. Ferris Jr. and N. C. Currie, "A Survey of Current Technologies for Through-The-Wall Surveillance (TWS)," Proc. SPIE, vol. 3577, pp. 62-72, Nov. 1998.

[2]   S. Nag, H. Fluhler, and M. Barnes, "Preliminary Interferometric Images of Moving Targets obtained using a Time-Modulated Ultra-Wide Band Through-Wall Penetration Radar," Proc. IEEE Radar Conference, pp. 64-69, May 2001.

[3]   N. C. Wild, F. Felber, M. Treadaway, F. Doft, D. Breuner, and S. Lutjens, "Ultrasonic Through-the-Wall Surveillance System," Proc. SPIE, Vol. 4232, pp. 167-176, 2001.

[4]   D. G. Falconer, K. N. Steadman, and D. G. Watters, "Through-the-Wall Differential Radar," Proc. SPIE, Vol. 2938, pp. 147-151, November 1996.

[5]   E. F. Greneker, "RADAR Flashlight for Through-the-Wall Detection Of Humans," Proc. SPIE, Vol. 3375, pp. 280-285, April 1998.

[6]   J. D. Black, "Motion and Ranging Sensor Through-the-Wall Surveillance System," Proc. SPIE, Vol. 4708, 2002, pp. 114-121.

[7]   A. R. Hunt, "Stepped-Frequency CW Radar for Concealed Weapon Detection and Through-The-Wall Surveillance," Proc. SPIE, Vol. 4708, 2002, pp. 99-105.

[8]   S. Nag, etal, "An Ultra-Wideband Through-the-Wall Radar for Detecting the Motion of People in Real Time," Proc. SPIE, Vol. 4744, pp. 48-57, 2002.

[9]   D. G. Falconer, R. W. Ficklin, K. G. Konolige, "Detection, Location, and Identification of Building Occupants using a Robot-Mounted Through-Wall Radar," Proc. SPIE, Vol. 4037, pp. 72-81, 2000.

[10]   F. Ahmad, G. J. Frazer, S. A. Kassam, M. G. Amin, "Design and Implementation of Near-field, Wideband Synthetic Aperture Beamformers," IEEE Trans. On Aerospace and Electronic Systems, Vol. 40, No. 1, pp. 206-220, Jan. 2004.

[11]   T. Sarkar, "Echo Cancellation using a Homomorphic Deconvolution," IEEE AP-S International Symposium and USNC/URSI National Radio Science Meeting, Monterey, Ca, June 2004.

[12]   A. Hurt, "Image Formation Through Walls using a Distributed Radar Sensor Network," IEEE AP-S International Symposium and USNC/URSI National Radio Science Meeting, Monterey, Ca, June 2004.

[13]   F. Ahmad, M. Amin, S. Kassam, "Synthetic Aperture Beamformer for Imaging Through a Dielectric Wall," Accepted for Publications in the IEEE Trans. On Aerospace and Electronic Systems.

[14]   F. Ahmad and S. Kassam, "Coarray Analysis of the Wide-Band Point Spread Function for Active Array Imaging," Signal Processing, vol. 81, pp. 99-115, Jan 2001.

[15]   G. Wang and M. Amin, "A New Approach for Target Location of Through-the-Wall Radar Imaging in the Presence of Wall Ambiguities," Proceedings of the IEEE International Symposium on Signal Processing and Information Technology, Rome, Italy, Dec. 2004.

[16]   G. Wang, M. Amin, and Y. Zhang, "A New Approach for Target Locations in the Presence of Wall Ambiguities," Submitted to the IEEE Trans. On Aerospace and Electronic Systems.

[17]   G. Mandapati and M. G. Amin, "Blurness and Focusing–Defocusing for Through-the-Wall Radar Imaging with Wall Ambiguities," Proceedings of the IEEE International Symposium on Signal Processing and Information Technology, Rome, Italy, Dec. 2004.

[18]   F. Ahmad and M. G. Amin, "A Noncoherent Radar System Approach for Through-The-Wall Imaging," SPIE Defense and Security Symposium, Conference on Homeland Security and Homeland Defense IV., Orlando, FL, March 2005.

[19]   W. Ailes, P. Rush, F. Ahmad, R. Dilsavor, W. Keichel, G. Titi, and M. Amin, "Experiments on Wideband Through the Wall Imaging," SPIE Defense and Security Symposium, Conference on Algorithms for SAR Imagery XII, , Orlando, FL, March 2005.